Galaxy-Independent Radial Structure of Dark Matter Halos

P. Steffen[1⋆]

[1]Deutsches Elektronen-Synchrotron DESY, Hamburg, Germany
⋆corresponding author: peter.steffen@desy.de

Abstract

We present an empirical analysis of the acceleration relation $g_{\rm obs}(g_{\rm bar})$ using the 2693 rotation-curve measurements of the 153 SPARC galaxies. The remaining residual scatter is consistent with the observational uncertainties, and no significant galaxy-dependent systematic deviations are observed.

We introduce a factorization of the radial distance r into a dimensionless coordinate $r_{\rm sc}$, which is independent of galaxy-to-galaxy differences, and a galaxy-dependent scale radius r_0. It allows the conversion of $g_{\rm bar}$ into the dimensionless coordinate $r_{\rm sc}$, ranging from zero (at the galactic center) to 1 (at the lowest values of measured $g_{\rm bar}$). The resulting $g_{\rm obs}(r_{\rm sc})$ is used to derive radial relations of the dark-matter mass and its volume density, and of the radial velocity distribution.

These relations characterize the radial structure of the galactic dark-matter halos as a function of $r_{\rm sc}$ independent of the galactic baryonic structure. The most important feature is a linear increase of dark-matter mass with $r_{\rm sc}$, starting at $r_{\rm sc} \approx 0.1$, up to a total enclosed mass of ≈ 6.5 times the galactic mass. It results in a mass density $\rho \propto r_{\rm sc}^{-2}$ in the range of the SPARC data. Further on, the radial distribution of the circular velocity shows an approach to a nearly constant value in the dark-matter dominated regime. The results suggest that the empirical acceleration relation reflects a common radial dark-matter structure shared by the SPARC galaxies. These results can serve as a selection criterion for viable halo models and dark-matter candidates.

1 Introduction

A large variety of halo models and fitting procedures have been applied to galaxy rotation curves, including NFW, Burkert, Einasto, and other parametrizations of the dark-matter (DM) distribution. Despite many successful studies, no single halo description has emerged as universally preferred for all galaxies (Li et al., 2020). This motivates an empirical analysis that reinvestigates the observational data themselves while minimizing prior assumptions about halo structure.

In the present work, we analyze the SPARC rotation-curve data within a dimensionless scaled radial framework that separates galaxy-dependent scaling from a common radial structure. The analysis aims to extract empirical regularities of the DM distribution directly from the observational data without assuming a specific halo profile. The resulting relations provide a consistent description of the SPARC measurements within their observational uncertainties.

McGaugh et al. (2016) have provided and analyzed the SPARC data, which are publicly available from the SPARC database `https://astroweb.case.edu/SPARC/`. The data consist of 2693 rotation-curve measurements from 153 late-type galaxies, including measurements of the baryonic acceleration $g_{\rm bar}$ and the observed centripetal acceleration $g_{\rm obs}$. A key result of this analysis is the discovery of a tight correlation between $g_{\rm obs}$ and $g_{\rm bar}$, which allows the calculation of $g_{\rm obs}$ from $g_{\rm bar}$:

$$g_{\rm obs}(g_{\rm bar}) = \frac{g_{\rm bar}}{1 - e^{-\sqrt{g_{\rm bar}/g_\dagger}}}, \tag{1}$$

where $\mathrm{g}_\dagger = 1.20 \cdot 10^{-10}$ m/s^2 is the fitted parameter, the acceleration value, where the discrepancy of $g_{\rm obs}$ and $g_{\rm bar}$ becomes pronounced. This parametrization provides a galaxy-independent description of the acceleration relation. The authors consider this as a minimalistic parametrization, that contains a linear slope at high accelerations and $g_{\rm obs} \propto \sqrt{g_{\rm bar}}$ at low accelerations. The empirical relation contains the full information required to determine the radial structure of the DM component once expressed in the scaled radial coordinate.

The SPARC data cover about two orders of magnitude, from $10^{-10}\ m/s^2$ to $10^{-12}\ m/s^2$.

In this analysis we use averages of binned data and least-squares fits. These are partly iterative processes in order to limit the deviations from the result to less than about 2.5 standard deviations (std). Data with no significant difference between $g_{\rm obs}$ and $g_{\rm bar}$ are not used in the fit.

2 Properties of the SPARC Data

The empirical acceleration relation $g_{\rm obs}(g_{\rm bar})$ forms the basis for the extraction of the radial structure of dark-matter (DM). In this section, we analyze the SPARC data in order to determine an accurate and unbiased empirical representation of this relation.

The SPARC data set provides 2693 rotation-curve measurements from 153 galaxies. We use the measured baryonic acceleration $g_{\rm bar}$ and the observed centripetal acceleration $g_{\rm obs}$, together with their uncertainties, to construct and test the empirical relation.

The original data, given in logarithms of the acceleration, are converted to accelerations in units of 10^{-12} m/s^2. The relative uncertainties, given in [dex] for the logarithmic values, are converted accordingly. Contrary to the logarithmic data the linear data are the preferred representation when investigating the differences of $g_{\rm obs}$ and $g_{\rm bar}$.

2.1 The Correlation between $g_{\rm bar}$ and $g_{\rm obs}$

McGaugh et al. (2016) have provided and analyzed the SPARC data. They found a strong correlation between $g_{\rm bar}$ and $g_{\rm obs}$ independent of mass and size of the galaxies (Equation 1). Although this parametrization captures the overall trend, the average residuals show a small but significant deviation from zero,

$$\delta g_{\rm fit} = (g_{\rm obs} - g_{\rm fit})/g_{\rm fit} = 0.082 \pm 0.005, \tag{2}$$

indicating a potential systematic bias.

Since this relation is used as the basis for deriving radial halo properties, an unbiased representation is required. We therefore determine an improved empirical least-squares fit of $g_{\rm obs}$ as a function of $g_{\rm bar}$ and $\sqrt{g_{\rm bar}}$. The resulting relation is given by

$$g_{\rm fit} = (9.77 \pm 0.27)\ \sqrt{g_{\rm bar}} + (0.77 \pm 0.03)\ g_{\rm bar}. \tag{3}$$

The quality of the fit results is $R^2 = 0.93$. A possible, additional constant term is compatible with zero (1.9 ± 2.1) and is omitted. Alternative parametrizations were tested but resulted in poorer fit quality.

The present formulation does not require an explicit acceleration scale as compared to the original RAR. Instead, the role of a characteristic acceleration scale is replaced by a continuous relation between baryonic and observed acceleration.

Figure 1 shows the scatter plot of the two variables as black points and the fitted curve as red line. The black line shows the values of $g_{\rm bar}$ indicating

the difference to $g_{\rm obs}$. The fluctuations of the single measurements around the fitted curve stay within a rather narrow band around the fitted curve.

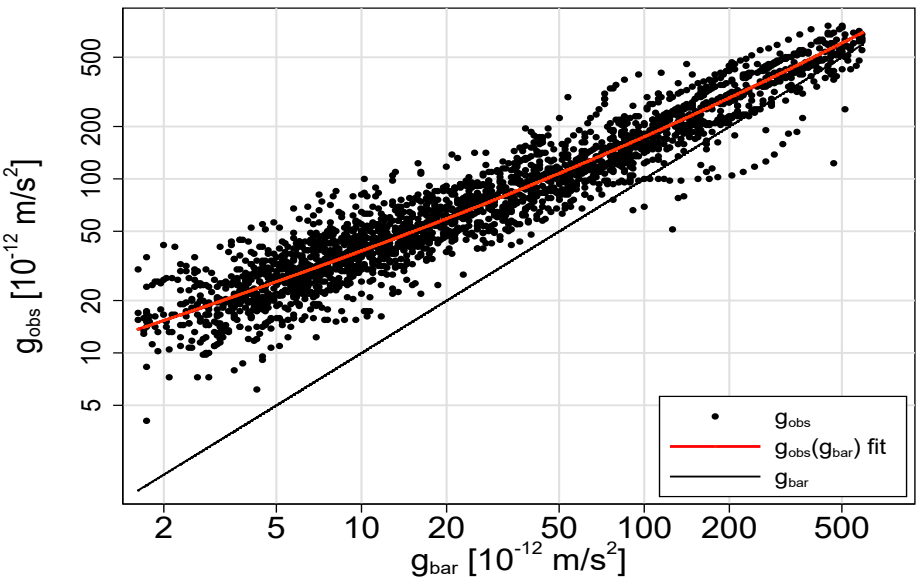

Figure 1: Scatter diagram of $g_{\rm obs}$ versus $g_{\rm bar}$ as black points and the fitted curve in red. The difference between $g_{\rm obs}$ and $g_{\rm bar}$ is indicated by the diagonal black line.

The average of the relative residuals is

$$\overline{\delta g_{\rm fit}} = \frac{\overline{(g_{\rm obs} - g_{\rm fit})}}{g_{\rm fit}} = 0.003 \pm 0.005 \quad (std = 0.25), \tag{4}$$

a value expected for an unbiased fit.

The standard deviation (std) is a measure of the fluctuation of the single residuals around zero. It agrees reasonably well with the slightly lower value of the average uncertainty of $\overline{\sigma g_{\rm obs}} = 0.23$. The small difference is consistent with a slight underestimation of the measurement uncertainties.

Possible contributions from uncertainties in $g_{\rm bar}$ are found to be negligible and do not introduce significant additional scatter in the $g_{\rm obs}$–$g_{\rm bar}$ relation.

Figure 2 shows a scatter plot of the the relative residuals $\delta g_{\rm fit}$ for the different $g_{\rm bar}$ values, as well as the distribution of $\delta g_{\rm fit}$. Two horizontal lines

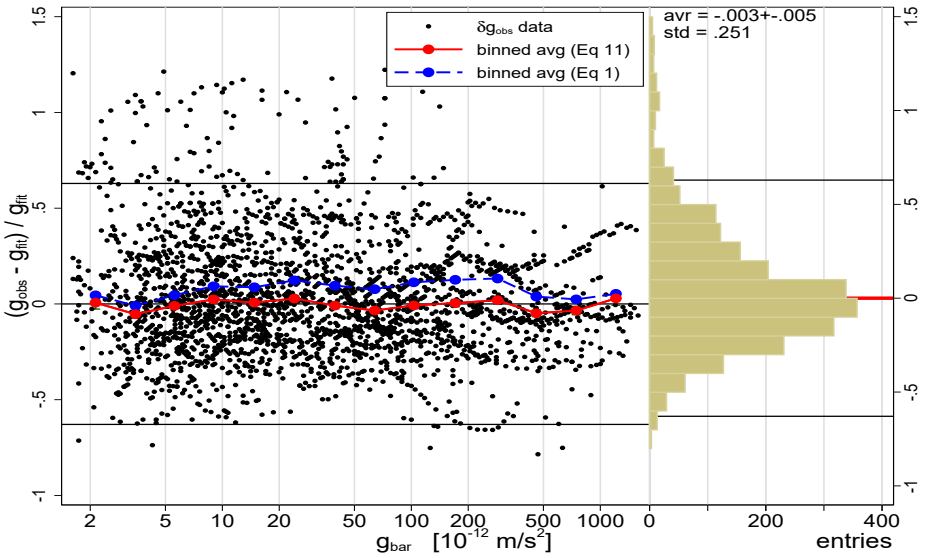

Figure 2: Scatter diagram of the relative fit residuals $\delta g_{\rm obs}(\rm fit)$ versus $g_{\rm bar}$ as black points. A projection onto the y-axis is shown on the right side. The stray points outside horizontal black lines are eliminated from the analysis. Averages of binned $g_{\rm bar}$-intervals are shown as thick red points. For comparison the blue points and dashed line indicate the average residuals of the RAR-fit (Equation 1).

mark the region of accepted data for fits and further averages.

The SPARC data provide also average values for 14 different equidistant logarithmic $g_{\rm bar}$ bins. The corresponding linear bin ranges are listed in Table 1, column 2, as well as the averages of $g_{\rm bar}$, $g_{\rm obs}$, $\delta g_{\rm obs}$, $g_{\rm fit}$, and $\delta g_{\rm fit}$ in columns 3 to 7. The average values of the relative fit residuals, $\delta g_{\rm fit}$, are shown in the scatter plot of Figure 2 as thick red points. They do not show a systematic trend within the $g_{\rm bar}$ range.

Figure 2 also shows, for comparison, the residuals of the original RAR parametrization (blue points), which exhibit a systematic deviation increasing with the $g_{\rm bar}$ values towards the point where the discrepancy of $g_{\rm obs}$ and $g_{\rm bar}$ becomes pronounced. This confirms the systematic bias indicated by Equation 2 and provides a direct justification for the use of the improved fit.

The possible influence of the galactic inner structure is expected to result

in differences between the averages increasing with $g_{\rm bar}$ resp a closer distance to the galactic center. This is not the case, neither for $\delta g_{\rm obs}$ nor for the std of $(g_{\rm obs} - g_{\rm fit})/g_{\rm fit}$. Instead, the agreement of $g_{\rm obs}$ with $g_{\rm fit}$ is excellent. Apart from bins 3 and 13, relative residuals of all bin values are less than 1 σ. Only bin 3 and 13 show a deviation from zero by 2.5 σ. They can be attributed to statistical fluctuations. An average of the std values of bins 5 to 14 of column 7 gives

$$\overline{std(\delta g_{\rm fit})} = 0.249 \pm 0.005 \quad (std = 0.015) \tag{5}$$

in good agreement with the value of 0.251 of equation 4.

In summary, the relation $g_{\rm obs}(g_{\rm bar})$ of Equation 3 provides a consistent and unbiased description of the SPARC data within the observational uncertainties. There is no indication of systematic galaxy-dependent deviations. It provides a robust basis for the derivation of a galaxy-independent radial structure in Section 3. This formulation does not introduce new empirical information beyond the acceleration relation itself, but provides a direct radial representation that makes the implied halo structure explicit.

Bin	$g_{\rm bar}$ range		$g_{\rm bar}$		$g_{\rm obs}$		$\delta g_{\rm obs}$	$g_{\rm fit}$	$(g_{\rm obs} - g_{\rm fit})/g_{\rm fit}$		
1	961.8	- 1573.7	1209.4	± 26.88	1309.7	± 52.82	0.32	1272.3	0.03	± 0.04	std= 0.24
2	587.8	961.8	745.4	11.77	813.6	22.50	0.30	841.6	-0.03	0.02	0.20
3	359.2	587.8	458.4	6.46	532.5	10.35	0.27	562.7	-0.05	0.02	0.18
4	219.6	359.2	286.0	3.60	391.4	8.33	0.28	385.8	0.02	0.02	0.24
5	134.2	219.6	170.8	1.91	260.4	5.67	0.22	259.4	0.00	0.02	0.26
6	82.0	134.2	103.1	1.10	177.2	3.54	0.20	178.7	-0.01	0.02	0.25
7	50.1	82.0	64.1	0.63	123.0	2.03	0.21	127.6	-0.03	0.01	0.21
8	30.6	50.1	39.4	0.38	90.7	1.58	0.22	91.7	-0.01	0.02	0.25
9	18.7	30.6	24.1	0.22	68.1	1.12	0.22	66.5	0.03	0.02	0.24
10	11.4	18.7	14.8	0.13	49.2	0.80	0.23	48.9	0.01	0.02	0.25
11	7.0	11.4	9.0	0.07	36.9	0.55	0.24	36.2	0.02	0.01	0.26
12	4.3	7.0	5.6	0.05	27.1	0.45	0.26	27.4	-0.01	0.02	0.27
13	2.6	4.3	3.5	0.04	19.7	0.43	0.24	20.9	-0.05	0.02	0.26
14	1.6	2.6	2.1	0.04	16.0	0.58	0.23	15.9	0.01	0.03	0.25

Table 1: $g_{\rm bar}$ bins (col 2) and the average values of $g_{\rm bar}$, $g_{\rm obs}$, $\delta g_{\rm obs}$, $g_{\rm fit}$ in columns 3 to 6. The relative fit residuals (col 7) are used to test the stability of the $g_{\rm obs}(g_{\rm bar})$ relation across acceleration ranges.

3 From Acceleration Relation to Radial Structure

The empirical $g_{\rm obs}(g_{\rm bar})$ relation of Equation 3 directly determines the $g_{\rm bar}$-dependence of the DM mass, density, and circular velocity.

The acceleration by the DM mass is $g_{\rm DM} = g_{\rm obs} - g_{\rm bar}$. The DM mass ratio of $m_{\rm DM}/M_{\rm bar}$ is obtained by

$$\frac{g_{\rm DM}}{g_{\rm bar}} = \frac{g_{\rm obs}(g_{\rm bar})}{g_{\rm bar}} - 1 = \frac{m_{\rm DM}}{M_{\rm bar}}, \tag{6}$$

resulting in

$$\frac{m_{\rm DM}}{M_{\rm bar}} = (9.77 \pm 0.27)\ /\sqrt{g_{\rm bar}} - (0.23 \pm 0.03). \tag{7}$$

It shows a linear increase of the DM mass ratio $\propto 1/\sqrt{g_{\rm bar}}$.

The observed centripetal acceleration is related to the circular velocity by

$$g_{\rm obs} = \frac{v_{\rm obs}^2}{r}. \tag{8}$$

resulting in

$$v_{\rm obs} = \sqrt{g_{\rm obs} r} = \sqrt{(9.77 \pm 0.27)\ \sqrt{g_{\rm bar}} + (0.77 \pm 0.03)\ g_{\rm bar}}\ \ \sqrt{r}. \tag{9}$$

Because of Newton's law

$$g_{\rm bar} = \frac{G M_{\rm bar}}{r^2}, \tag{10}$$

$\sqrt{g_{\rm bar}}$ is a kind of inverse measure for the distance from the galactic center. However, $g_{\rm bar}$ is correlated to the two parameters $M_{\rm bar}$ and the radial distance r, which can vary independently. This ambiguity is resolved by splitting r into two components: a radius r_0 for a fixed baryonic acceleration g_0, and a dimensionless distance $r_{\rm sc}$, ranging from zero (at the galactic center) to one (at $g_{\rm bar} = g_0$). We have used a value of $g_0 = 2\ 10^{-12}$ m/s^2, about the smallest measured value of $g_{\rm bar}$, such that $r_{\rm sc}$ covers the full range of available acceleration measurements.

$$r_0 = \sqrt{\frac{G M_{\rm bar}}{g_0}} \tag{11}$$

$$r_{\rm sc} = \sqrt{\frac{g_0}{g_{\rm bar}}} \tag{12}$$

$$r = r_0 \cdot r_{\rm sc} \tag{13}$$

Although disk galaxies exhibit extended baryonic mass distributions, the scaling radius r_0 is defined through the total baryonic mass $M_{\rm bar}$ and therefore represents a global property of the system. The contribution of outer disk regions to $Mbar$ and with it to r_0 is subdominant. Therefore r_0 provides a global normalization of the radial coordinate. It is largely insensitive to the detailed radial distribution of baryonic matter.

The relation $g_{\rm obs}(g_{\rm bar})$ of Equation 3 is used to derive the corresponding radial distributions. Equation 12 is used to convert the $g_{\rm bar}$-dependence into a dependence on the scaled radial coordinate $r_{\rm sc}$.

$$r_{\rm sc} = \frac{r}{r_0} = \sqrt{\frac{2\ 10^{-12}\ {\rm m/s^2}}{g_{\rm bar}}}. \tag{14}$$

Using Equation 14, the fit relation of Equation 3 can be rewritten as a function of $r_{\rm sc}$:

$$g_{\rm fit}(r_{\rm sc}) = \frac{13.82 \pm 0.38}{r_{\rm sc}} + \frac{1.54 \pm 0.05}{r_{\rm sc}^2}. \tag{15}$$

For the different galaxies the r-ranges differ because of Equation 13.

The radial dependence of Equations 7 is

$$m_{\rm DM}/M_{\rm bar}(r_{\rm sc}) = (6.91 \pm 0.19) \cdot r_{\rm sc} - (0.229 \pm 0.027). \tag{16}$$

It shows a constant increase of the DM mass starting at $r_{\rm sc} \approx 0.1$. An extrapolation towards $r_{\rm sc} = 0.$ is not constrained and the relation could flatten towards small radii. For the different galaxies the r-ranges differ because of Equation 13.

Equation 16 formally extrapolates to a vanishing DM contribution at $r_{\rm sc} \approx 0.033$. However, the extrapolation towards smaller radii is not constrained by the present data and the relation may flatten towards the galactic center. A clearly visible DM contribution emerges at $r_{\rm sc} \gtrsim 0.1$, while the DM component becomes dominant over the baryonic contribution for $r_{\rm sc} \gtrsim 0.2$, corresponding to $m_{\rm DM}/M_{\rm bar} \gtrsim 1$.

The DM mass density $\rho_{\rm DM}$ is the differential quotient

$$\rho_{\rm DM}(r_{\rm sc}) = \frac{d\ m_{\rm DM}/M_{\rm bar}(r_{\rm sc})}{d\ V(r_{\rm sc})} = \frac{d\ m_{\rm DM}/M_{\rm bar}(r_{\rm sc})/d\ r_{\rm sc}}{d\ V(r_{\rm sc})/d\ r_{\rm sc}} \tag{17}$$

The numerator, $d\ m_{\rm DM}/M_{\rm bar}(r_{\rm sc})/d\ r_{\rm sc} = (6.91 \pm 0.19)$, is obtained from Equation 16, while the denominator is the differential shell volume, $d\,V(r_{\rm sc})/d\,r_{\rm sc} = 4/3\ \pi\ d\ r_{\rm sc}^3 = 4\ \pi\ r_{\rm sc}^2\ d\ r_{\rm sc}$.

The result is

$$\rho_{\rm DM}(r_{\rm sc}) = (0.550 \pm 0.015)/r_{\rm sc}^2, \tag{18}$$

a $r_{\rm sc}^{-2}$ dependency of the DM mass density. For the different galaxies the r-ranges differ because of Equation 13.

Using $r = r_{\rm sc} r_0$, we obtain from Equation 9

$$v_{\rm obs}(r) = \sqrt{g_{\rm obs} r} = \sqrt{g_{\rm obs} r_{\rm sc}}\sqrt{r_0} = v_{\rm u}\sqrt{r_0} \quad \text{with} \tag{19}$$

$$v_{\rm u}(r_{\rm sc}) = \sqrt{(13.82 \pm 0.38) + (1.54 \pm 0.05)/r_{\rm sc}}. \tag{20}$$

The unified velocity ($v_{\rm u}$) describes the shape of the velocity distribution independent of the galactic mass, while $\sqrt{r_0}$ serves as specific galactic scale for $v_{\rm obs}$.

Thus, the relation $g_{\rm obs}(g_{\rm bar})$ contains the full information required to determine the radial structure of the data when expressed in an appropriate radial coordinate.

The data have been averaged for the different $g_{\rm bar}$ bins, which are then converted into $r_{\rm sc}$ bins. The results are listed in Table 2. The different radial distribution of the averages are shown in Figure 3 together with the corresponding fit result The statistical errors of the averages are covered by the thickness of the red points. The shown error bars show the std of the averages indicating the fluctuations of the single measurements. (Equations 15, 16, 18, and 20) are shown as red curves. The agreement between averages and the curves obtained from the corresponding Equation 3 is very good.

bin	$r_{\rm sc}$ range		$r_{\rm sc}$	$g_{\rm obs}$		$m_{\rm DM}$		ρ		$v_{\rm u}$	
1	0.036	- 0.043	0.039	1309.72	±52.82	0.08	± 0.04	356.69	± 9.91	7.24	± 0.13
2	0.043	0.055	0.049	813.64	22.50	0.09	0.02	227.96	6.34	6.44	0.08
3	0.055	0.070	0.063	532.55	10.35	0.17	0.02	139.07	3.87	5.91	0.05
4	0.070	0.090	0.080	391.41	8.33	0.38	0.03	85.52	2.38	5.69	0.06
5	0.090	0.115	0.103	260.39	5.67	0.53	0.03	52.22	1.45	5.26	0.05
6	0.115	0.147	0.131	177.16	3.54	0.73	0.03	31.86	0.89	4.93	0.05
7	0.147	0.189	0.168	123.01	2.03	0.93	0.03	19.40	0.54	4.64	0.03
8	0.189	0.241	0.216	90.69	1.58	1.32	0.04	11.84	0.33	4.49	0.04
9	0.241	0.310	0.276	68.11	1.12	1.86	0.05	7.21	0.20	4.41	0.04
10	0.310	0.396	0.354	49.20	0.80	2.36	0.05	4.40	0.12	4.22	0.03
11	0.396	0.504	0.451	36.93	0.55	3.16	0.06	2.70	0.08	4.15	0.03
12	0.504	0.647	0.577	27.06	0.45	3.89	0.08	1.65	0.05	3.99	0.03
13	0.647	0.824	0.738	19.74	0.43	4.73	0.12	1.01	0.03	3.83	0.04
14	0.824	1.110	0.971	15.99	0.58	6.57	0.25	0.58	0.02	3.91	0.07

Table 2: Averages determined for different $g_{\rm bar}$ bins. Columns list the $r_{\rm sc}$ range used for the bin averages, the mean scaled radius $r_{\rm sc}$, and the averages of $g_{\rm obs}$, the enclosed DM mass ratio $m_{\rm DM}/M_{\rm bar}$, the shell density ρ, and the unified velocity $v_{\rm u}$.

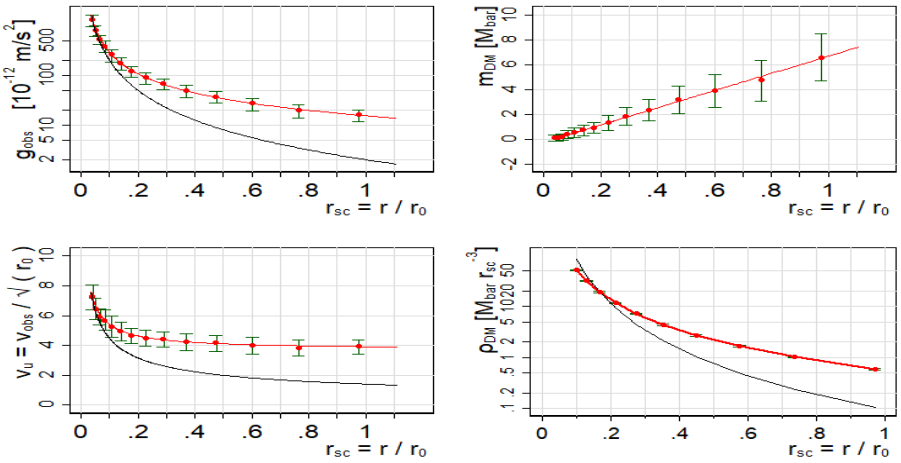

Figure 3: Radial distributions of $g_{\rm obs}$ (top left), $v_{\rm u}$ (bottom left), $m_{\rm DM}/M_{\rm bar}$ (top right), and $\rho_{\rm DM}$ (bottom right). Shown are the averages of the different $g_{\rm bar}$ bins as red points with std as error bars. Red lines show the results corresponding to the $g_{\rm obs}(g_{\rm bar})$ fit. The black lines indicate comparison distributions without a dark-matter contribution and, in the case of $\rho_{\rm DM}(r_{\rm sc})$, a comparison slope corresponding to an $r_{\rm sc}^{-3}$ dependence. In case of the $\rho_{\rm DM}(r_{\rm sc})$ the error bars indicate the uncertainty of the $m_{\rm DM}/M_{\rm bar}$ slope.

3.1 Summary of the Radial Structure

The transformation to the scaled radial coordinate $r_{\rm sc}$ reveals a common radial structure of the SPARC galaxies independent of their individual masses and sizes. The principal empirical properties are:

1. The DM contribution emerges at $r_{\rm sc} \gtrsim 0.1$ and dominates over the baryonic contribution for $r_{\rm sc} \gtrsim 0.2$.

2. The enclosed DM mass increases linearly with radius,

$$m_{\rm DM}/M_{\rm bar}(r_{\rm sc}) \propto r_{\rm sc}, \tag{21}$$

   corresponding to a constant increase of the DM mass within the observed SPARC range.

3. The enclosed DM mass reaches a value of $m_{\rm DM} \approx 6.5\ M_{\rm bar}$ within the observed SPARC range.

4. The corresponding density profile follows

$$\rho_{\rm DM}(r_{\rm sc}) \propto r_{\rm sc}^{-2}, \tag{22}$$

   consistent with an isothermal-like halo structure.

5. The unified circular velocity $v_{\rm u}(r_{\rm sc})$ approaches an approximately constant value in the DM dominated regime.

These properties emerge directly from the empirical acceleration relation once expressed in the scaled radial coordinate. The radial properties of individual galaxies can be obtained by using Equation 13.

4 Discussion

The analysis is limited to the radial range covered by the SPARC data, and the behavior at larger radii remains unconstrained. Likewise, the extrapolation towards very small $r_{\rm sc}$ is not constrained by the present data and may deviate from the linear relation. The present work therefore identifies the common radial structure within the observed SPARC range, but does not constrain the inner or outer halo boundaries.

The results are based on the empirical relation $g_{\rm obs}(g_{\rm bar})$ and do not address the underlying physical origin of this relation. Future observations extending to larger galactocentric distances, as well as theoretical models capable of reproducing the observed scaling behavior, will be required to clarify the physical origin of the observed halo structure.

4.1 Origin of the Empirical Acceleration Relation

The empirical acceleration relation $g_{\rm obs}(g_{\rm bar})$ describes the SPARC data with high accuracy. However, its physical origin is not directly evident from the acceleration correlation itself.

The transformation to the scaled radial coordinate $r_{\rm sc}$ reveals that the acceleration relation is one-to-one connected to the radial dependence of the enclosed DM mass ratio $m_{\rm DM}/M_{\rm bar}(r_{\rm sc})$ (Equation 16), shown in upper-right panel of Figure 3. The linear rise of the enclosed DM mass with $r_{\rm sc}$, common to all 153 SPARC galaxies within the observational uncertainties, defines a galaxy-independent radial halo structure.

In this interpretation, the empirical acceleration relation is not the primary physical relation itself, but rather a consequence of the common radial DM structure shared by the SPARC galaxies.

4.2 Comparison to different Models

The inferred density profile $\rho_{\rm DM} \propto r^{-2}$ corresponds to an isothermal-like halo structure (Bahcall & Soneira, 1980; Binney & Tremaine, 2008). Navarro–Frenk–White halos (Navarro et al., 1997) exhibit a $\rho \propto r^{-2}$ behaviour only near their characteristic scale radius and steepen to $\rho \propto r^{-3}$ at larger radii. Burkert profiles (Burkert, 1995) generally predict declining outer rotation curves. The present analysis therefore provides a model-independent empirical benchmark against which such halo models can be compared.

5 Conclusion

We have shown that the radial structure of DM halos can be derived directly from the empirical acceleration relation $g_{\rm obs}(g_{\rm bar})$ by introducing a scaled radial coordinate $r_{\rm sc} = r/r_0$. This transformation removes galaxy-to-galaxy scaling differences within the resolution of the present data and reveals a unified, galaxy-independent halo structure. The scaling radius r_0 depends on the total baryonic mass and provides a global normalization of the radial coordinate. In this sense, the resulting scaled coordinate is largely insensitive to the detailed radial distribution of baryonic matter, allowing the intrinsic DM structure to be extracted in a model-independent way.

Within this framework, the principal empirical properties of DM halos follow as direct consequences of the observed acceleration relation:

1. **Emergence of DM effects:** The DM contribution emerges at $r_{\rm sc} \gtrsim 0.1$ and exceeds the baryonic contribution for $r_{\rm sc} \gtrsim 0.2$.

2. **Mass growth:** The enclosed DM mass increases linearly with radius,

$$\frac{m_{\rm DM}}{M_{\rm bar}} = (6.9 \pm 0.2)\, r_{\rm sc} - (0.23 \pm 0.03),$$

   leading to a total enclosed ratio

$$\frac{M_{DM}}{M_{\rm bar}} = 6.5 \pm 0.2.$$

   This result makes explicit the halo structure that is only implicitly contained in the empirical acceleration relation.

3. **Density profile:** The derived $\rho_{\rm DM}(r_{\rm sc}) \propto r_{\rm sc}^{-2}$ indicates an isothermal-like halo structure.

4. **Kinematic evidence:** The unified circular velocity $v_{\rm u}$ approaches a constant value asymptotically, with a residual radial dependence at finite $r_{\rm sc}$.

The transformation to the scaled radial coordinate further suggests that the empirical acceleration relation is directly connected to the common radial DM structure shared by the SPARC galaxies. In this interpretation, the acceleration relation reflects the common radial growth of the enclosed DM mass revealed by the scaled radial analysis.

The present analysis provides a model-independent empirical description of the radial structure of DM halos within the radial range covered by the SPARC data. The inferred profiles are consistent with an isothermal-like halo structure and provide direct empirical constraints for theoretical halo models such as NFW and Burkert profiles. Future observations extending to larger galactocentric radii will be required to test the persistence of the observed scaling relations and to clarify the physical origin of the empirical acceleration relation.

Data availability

The data underlying this article are publicly available from the SPARC database at `https://astroweb.case.edu/SPARC/`.

Acknowledgment

I thank the DESY Directorate and the IT division for their continuous support. I am grateful for the productive discussions with the GRAVI group at DESY, G. Schierholz, U. Martyn, and K. Schmidt-Hoberg. Special thanks go to the SPARC collaboration for providing the astronomical data on which this analysis is based.

References

Bahcall J., Soneira R., 1980, Astrophys. J. Suppl., 44, 73

Binney J., Tremaine S., 2008, Galactic Dynamics, 2 edn. Princeton University Press

Burkert A., 1995, Astrophys. J. Lett., 447, L25

Li P., Lelli F., McGaugh S., Schombert J., et al., 2020, Astrophysical Journal Supplement Series, 247, 31

McGaugh S., Lelli F., Schombert J., 2016, Phys. Rev. Lett., 117, 201101

Navarro J. F., Frenk C. S., White S. D. M., 1997, Astrophys. J., 490, 493